Korean J. Chem. Eng., 38(4), 747-755 (2021)
DOI: 10.1007/s11814-020-0736-6

pISSN: 0256-1115
eISSN: 1975-7220

Highly dispersed Cu-ZnO-ZrO_2 nanoparticles on hydrotalcite adsorbent as efficient composite catalysts for CO_2 hydrogenation to methanol

Xin Fang*,, Yuhan Men**, Fan Wu**, Qinghu Zhao**, Ranjeet Singh**, Penny Xiao**, Liying Liu*, Tao Du*,†, and Paul A. Webley**,†**

*State Environmental Protection Key Laboratory of Eco-Industry, Northeastern University, Shenyang 110819, China
**Department of Chemical Engineering, The University of Melbourne, Parkville, VIC 3010, Australia
(*Received 22 September 2020 • Accepted 23 December 2020*)

Abstract−CO_2 hydrogenation to methanol is attracting specific interest because of its potential economic and environmental benefits in transforming waste CO_2 to value-added hydrocarbons. Copper-based catalysts are documented as efficient and widely applied, whereas insufficient catalytic properties of conventional catalysts hinder their application. Herein, catalysts using Mg-Al hydrotalcite (HT) as the carrier of Cu/ZnO/ZrO_2 (CZZ) nanoparticles were prepared to exploit special advantages of hydrotalcite on copper dispersion and catalytic performance. The results show that CZZ nanoparticles can be uniformly dispersed on external surfaces of HT, elevating BET surface areas of CZZ-HT samples by at least 2.5 times compared to pure CZZ. The HT carrier also enriches strong basic sites and hence elevates CO_2 adsorption capabilities in the range of reaction temperature. Both copper surface area and copper dispersion of CZZ-HT samples are improved dramatically. A catalyst containing 45.1 wt% of CZZ shows 1.1 times higher copper surface area per gram CZZ and 1.6 times higher copper dispersion than the reference CZZ. Subsequent reactions demonstrate the CZZ-HT samples show remarkably promoted turnover frequency (TOF) for methanol synthesis and retain considerable catalyst stability. The typical catalyst prepared in this research, at the reaction temperature of 523 K and pressure of 3.0 MPa, presents a 68.2% higher methanol STY_{Cu} per gram copper and an 117.0% higher S_{MeOH}/S_{CO} ratio than the commercial catalyst. The support HT plays a crucial role for the enhanced catalytic performance physically and chemically. Thus, the as-prepared CZZ-HT catalyst provides a significant improvement for CO_2 utilization.

Keywords: CO_2, Hydrogenation, Methanol, Hydrotalcite, High Dispersion

INTRODUCTION

Unprecedented worldwide attention has been paid recently to CO_2 conversion to cope with the increasing crisis of climate change. As one of many CO_2 utilization techniques, CO_2 hydrogenation to methanol (CH_3OH, viz., MeOH) is especially interesting due to its intermediate position in the promising carbon neutral cycle [1-3]. The produced methanol is an appropriate medium connecting waste CO_2 and value-added hydrocarbons, such as dimethyl ether (DME) [4], light olefins [5] and gasoline [6].

The improvement of catalysts for use in CO_2 hydrogenation is ongoing, but there remain many restrictions to current performance, including low methanol selectivity and CO_2 conversion at moderate reaction conditions [7,8]. One primary approach to improve the catalytic performance involves developing novel catalysts with active components such as transition metals and precious metals. For example, the Ni_5Ga_3 catalyst supported on silica was reported for use in CO_2 hydrogenation at ambient pressure, providing excellent methanol+DME selectivity of over 95% within the temperature range of 433 to 503 K [9,10]. A Pd/In_2O_3 catalyst showed good methanol selectivity with over 70% at a temperature of 573 K and a pressure of 5 MPa [11]. Gold nanoparticles activated on a CeO_x/TiO_2 interface also improved methanol selectivity to ~60% at 573 K [12]. Alternatively, it is also approval to fine-tune the catalytic metal interface by importing additives to copper-based catalysts. Well-known additives include zinc, aluminium, zirconium, which can improve the reactivity and stability simultaneously [13-20].

The emerging single-atom catalysis is a promising trend for catalyst development recently [21-23]. It is widely acknowledged that the catalytic activity of catalyst can be enhanced with the facilitated dispersion of active component. In conventional copper-based catalysts, however, the dispersion of active copper is usually as low as approximately 20% [24-27], so most of the copper atoms do not serve as active sites. Thus, dramatic improvement in catalytic property can be expected if we elevate the copper surface area and dispersion. For this purpose, Mg-Al hydrotalcite (HT) is an ideal supporting material for active metals because of its favorable characteristics, such as high specific surface area, reversible layered double structure and maintained CO_2 adsorption capacity at a moderate temperature range around 523 K [28-30]. In our previous work [31], we preliminarily confirmed the superiority of HT as the carrier to improve methanol yield and selectivity, but the mechanism of how HT influences the overall textural structures and catalytic properties remains to be further investigated.

In the present work, HT supported catalysts with various CZZ contents (CZZ-HTs) were prepared via a mild method. Components, structures and morphologies of CZZ-HT samples were analyzed by characterization of XRD, SEM-EDX, and low-temperature

†To whom correspondence should be addressed.
E-mail: dut@smm.neu.edu.cn, paul.webley@unimelb.edu.au

N_2 adsorption-desorption. Surface active sites of catalysts were then tested by H_2-TPR and CO_2-TPD, followed by measurement of copper surface area and dispersion by N_2O titration. Catalytic performance of the CZZ-HT samples during CO_2 hydrogenation was investigated on a fixed-bed reactor and compared with conventional CZA and CZZ catalysts. The mechanism was also explored and discussed based on HIM, HRTEM, etc.

EXPERIMENTAL

1. Preparation of CZZ-HT Catalyst

CZZ-HT catalysts with different CZZ contents were synthesized via the ultrasonic assisted co-deposition (UACD) method. Prior to preparation, the carrier, hydrotalcite (Pural MG50, SASOL), was activated in air at 673 K for 4 h with a ramp rate of 1 K min^{-1} (see Reagents in SI). In a typical preparation process, 3 g of activated HT was uniformly dispersed in 12.5 mL of CZZ ternary nitrate solution, and the suspension was ultrasonicated for 5 min and stirred for 2 h. A solution of 1.2 M K_2CO_3 was dropwise added (3 mL min^{-1}) under continuous stirring until the pH reached ~9.5, followed by 2 h of stirring and 1 h of aging. The as-obtained mixture was filtered, washed with deionized water, and dried at 393 K overnight. To prepare catalyst products, the dried powders were calcined at 673 K for 4 h in air. CZZ content in samples was controlled by varying the initial concentration of total ternary metal nitrate as 0.3, 0.9, 1.5 and 2.1 M, respectively, and the corresponding samples were labelled as 1CZZ-HT, 3CZZ-HT, 5CZZ-HT and 7CZZ-HT.

2. Characterization

Chemical composition of CZZ-HT samples was measured by inductive coupled plasma emission spectrometer (ICP-OES; Varian 720ES, Agilent).

Crystal structure was determined by powder X-ray diffraction equipped with a Cu-Kα radiation (PXRD; PW1140/90, Phillips Analytical). The scan range was 2θ=25-70° with a step of 0.02°.

Morphology, surface metal distribution and chemical composition were analyzed by scanning electron microscope and energy dispersive spectroscopy (SEM-EDX; JSM-7001F, JEOL). Samples were coated with a thin layer of gold prior to analyze.

N_2 adsorption-desorption isotherms were measured at 77 K (BELSORP-max, MicrotracBEL) to calculate the Brunauer-Emmett-Teller (BET) surface area. Each sample was fully vacuum degassed at 373 K for 3 h and at 573 K for 3 h before measurement.

Reducibility was measured by hydrogen temperature programmed reduction (H_2-TPR; BELCAT-M, MicrotracBEL). The sample was pre-calcined at 573 K in Ar (Coregas) flow for 3 h to remove adsorbed H_2O, CO_2, etc. After cooling to 373 K, it was heated in 5% H_2 flow (balanced with Ar, Coregas) from 323 to 973 K with a ramp rate of 5 K min^{-1}. The H_2 consumption was recorded by mass spectrometry (BELMass, MicrotracBEL) [32].

Basic sites were studied by CO_2 temperature programmed desorption (CO_2-TPD; BELCAT-M, MicrotracBEL). The reduced sample was held at 573 K for 3 h in Ar (Coregas) flow to remove adsorbed molecules and then treated by 5% CO_2 (balanced with He, Coregas) at 393 K for 1 h. At such temperatures, the CO_2 adsorption occurred on basic sites of the samples. The temperature was afterwards increased to 750 K (5 K min^{-1}) in Ar (Coregas) flow so that CO_2 adsorbed in the sample was desorbed. The desorbed CO_2 was also detected by the mass spectrometry (BELMass, MicrotracBEL).

A two-step N_2O titration method was adopted to analyze the copper surface area and copper dispersion (BELCAT-M, MicrotracBEL) of the samples [33,34]. First, the sample was reduced in 5% H_2 (balanced with Ar, Coregas) at 573 K for 6 h. When it cooled to the ambient temperature, the reduced sample was weighted and reinstalled in the apparatus. Afterwards, it was exposed to 5% N_2O (balanced with He, Coregas) at 333 K for 1 h to oxidize its surface Cu^0 to Cu_2O [35] and reduced again in 5% H_2 with increasing temperature from 333 to 623 K (5 K min^{-1}). The H_2 consumption during both processes was recorded by mass spectrometry (BELMass, MicrotracBEL), and parameters were calculated by assuming a Cu/N_2O stoichiometry of 2 and an atomic copper surface density of 1.46×10^{19} atoms m^{-2} [36,37].

Microstructure of the reduced sample with high resolution was analyzed with helium ion microscopy (HIM; ORION NanoFab, Carl Zeiss) and high resolution transmission electron microscope operated at 200 kV (HRTEM; JEOL 2010).

3. Catalysis Experiments

Catalytic experiments were conducted within a fixed bed reactor (see Micro-Reactor and Fig. S1 in the SI) equipped with a gas chromatograph (GC; GC7890B, Agilent)[31]. Typically, 1 g of the well mixed tableted sample (diameter of 0.2-0.5 mm) and 1 g of quartz sand (50-70 mesh, Sigma-Aldrich) were filled in the column (Ø10×500 mm) and were reduced by pure H_2 (Coregas) at 573 K for 6 h within the reactor. After cooling to the ambient temperature in N_2 (Coregas) flow, the column was heated and maintained at a set temperature. The system pressure was maintained by a backpressure regulator. The inlet flowrate of pre-mixed gas (24.7% CO_2 balanced with H_2, BOC) was regulated by a mass flow controller (5850E, Brooks) so that catalytic reactions proceeded at well controlled conditions. Flowrates of off-gas were measured by a bubble flowmeter (Sigma-Aldrich) and components were analyzed by the GC every 2 h until the reaction reached equilibrium. Volume and mass of catalyst were finally quantified after reactions.

CO_2 conversion (X_{CO_2}, %), product selectivity (S_{MeOH} and S_{CO}, %), space time yield (STY, $mg_{MeOH}\ g_{catalyst}^{-1}\ h^{-1}$ and $mg_{MeOH}\ g_{Cu}^{-1}\ h^{-1}$) and turnover frequency (TOF, s^{-1}) were calculated to clarify catalytic properties of the samples (see Reaction Parameter Calculations in SI).

RESULTS AND DISCUSSION

1. Structures and Morphologies

Chemical composition of CZZ-HT samples after calcination of precursors was obtained from ICP and summarized in Table 1. Every sample contains metal elements of magnesium, aluminium, copper, zinc and zirconium, in which the first two are structural metals of the layered double frameworks of HT and the remaining ones serve as active constituents for CO_2 hydrogenation. Consistent with the sample labels, the CuO-ZnO-ZrO_2 content increases from 1CZZ-HT to 7CZZ-HT, and thus the loading rate of CZZ in samples are well controlled.

Table 1. Chemical composition of 1CZZ-TH, 3CZZ-HT, 5CZZ-HT and 7CZZ-HT (wt%)

	Mg	Al	Cu	Zn	Zr	CuO-ZnO-ZrO_2
1CZZ-HT	24.9	23.0	3.6	6.0	3.0	15.2
3CZZ-HT	14.9	21.0	10.3	14.3	5.4	35.4
5CZZ-HT	14.6	16.8	17.2	14.3	6.7	44.0
7CZZ-HT	12.5	10.2	23.0	21.2	7.7	59.8

Fig. 1(a) shows XRD patterns of samples before reduction. Two categories of diffraction peaks can be classified: amorphous HT and crystalline metal oxides (refer to Fig. S2 in SI). The amorphous HT presents three broad peaks at 2θ=35.6, 43.4 and 62.8°, whereas the metal oxides mainly include peaks of CuO (JCPDS 45-0937) and ZnO (JCPDS 36-1451). When the CZZ content increases from 1CZZ-HT to 7CZZ-HT, peaks of the amorphous HT gradually weaken, whereas peaks of metal oxides are strengthened. No peak related to Zr can be detected as reported in other CZZ catalyst studies because of its weak signal [38,39]. The identical crystal phases evidenced by XRD patterns confirm similar crystal texture of prepared CZZ-HT samples.

These samples, however, present visible differences in morphology according to SEM images. As shown in Fig. 1(b), the 1CZZ-HT perfectly inherits the morphology of activated HT with a nanoflower appearance (see Fig. S3 in the SI), ensuring it abundant external surfaces on which tiny nanoparticles can be observed. Sample 3CZZ-HT (Fig. 1(c)) and 5CZZ-HT (Fig. 1(d)) contain more nanoparticles on their external surfaces as the CZZ content rises. However, when the CZZ content reaches a high level of 65 wt%, i.e., 7CZZ-HT shown in Fig. 1(e), the surface metal oxide concentration is too high to form particle agglomeration. As supplemented by EDX images (Fig. 1(b)-(e)), metal elements of copper, zinc and zirconium disperse evenly in all samples except 7CZZ-HT. In 7CZZ-HT, several bright spots appear in its EDX image of copper, demonstrating the presence of metal agglomeration which inhibits copper dispersion.

Table 2. Surface areas and pore diameters of samples before and after reduction

	BET surface area ($m^2\ g^{-1}$)	Average pore diameter (nm)
HT	195.2	5.06
1CZZ-HT	184.0	6.90
3CZZ-HT	155.0	8.24
5CZZ-HT	138.6	13.23
7CZZ-HT	126.1	11.95
r1CZZ-HT	133.9	7.88
r3CZZ-HT	136.0	8.70
r5CZZ-HT	119.5	14.40
r7CZZ-HT	109.8	13.93

BET surface areas of CZZ-HT samples also vary with the CZZ content as listed in Table 2 and the introduction of HT enlarges the BET surface area of CZZ-HT samples. The higher the CZZ content, the lower the BET surface area. For the average pore diameter, the pore diameter of blank HT is only 5.06 nm due to its narrow interlayer spacing [40], whereas that of CZZ is usually large because of interparticle pores [41]. With elevated CZZ content, the pore diameter is generally enlarged due to interparticle pores (see Fig. S4 in SI). Nevertheless, the 7CZZ-HT presents reduced pore diameter as a consequence of particle agglomeration. Table 2 further shows that BET surface areas of the catalysts, though retaining the same trend as samples before reduction, decrease after reduction because the new generated phase of Cu^0 sinters upon exposure to a reducing environment [15].

2. Surface Active Sites

Since all CZZ-HT samples present favorable thermal stability

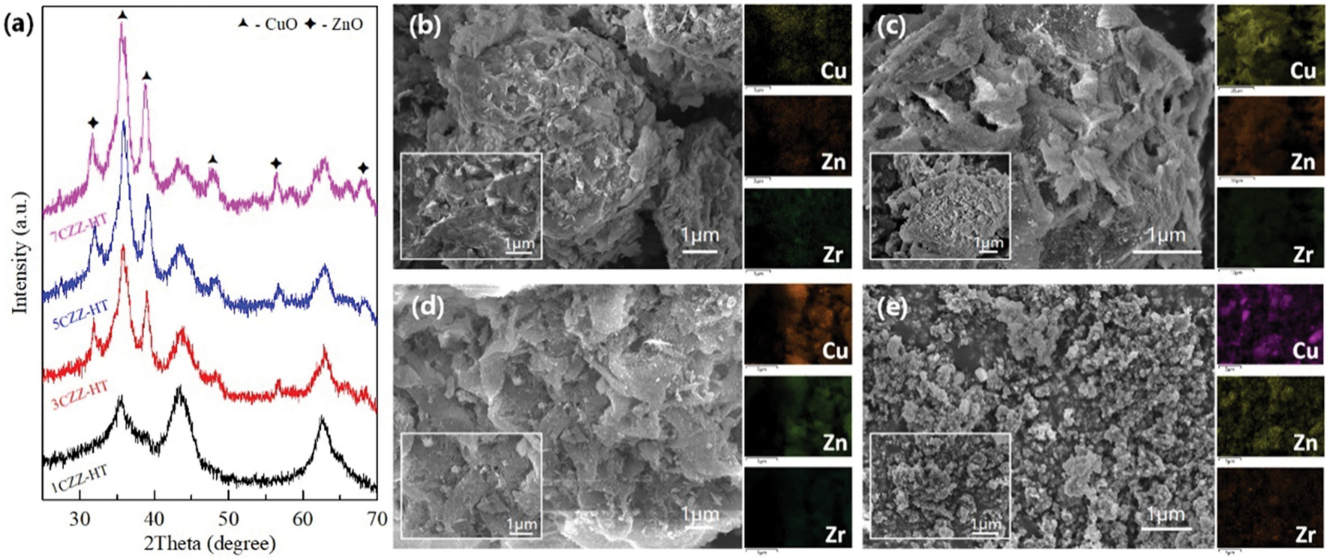

Fig. 1. (a) XRD patterns of 1CZZ-TH, 3CZZ-HT, 5CZZ-HT and 7CZZ-HT. SEM-EDX images of (b) 1CZZ-HT, (c) 3CZZ-HT, (d) 5CZZ-HT and (e) 7CZZ-HT.

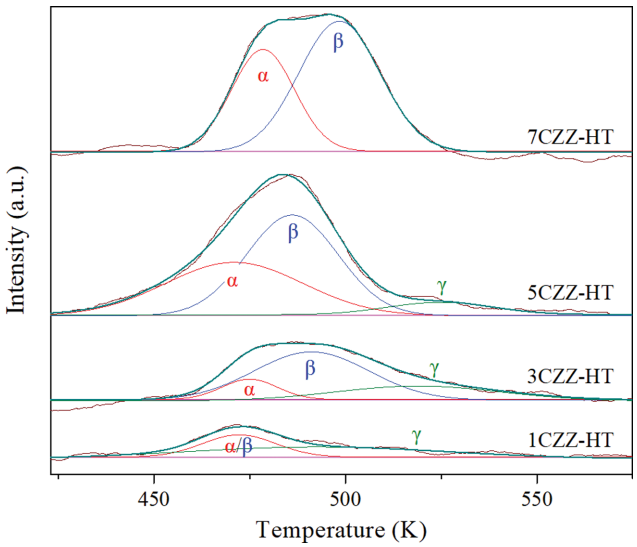

Fig. 2. H_2-TPR profiles of 1CZZ-TH, 3CZZ-HT, 5CZZ-HT and 7CZZ-HT.

up to a temperature of at least 700 K (see Thermal Stability Analysis and Fig. S5 in SI), they can be reduced below this temperature without destroying their structure. The copper status in the samples can be identified by H_2-TPR [42]. Fig. 2 suggests three types of reducible copper compounds in samples: isolated copper oxide, copper combined with ZnO and ZrO_2, and copper combined with HT, corresponding to peaks α, β and γ, respectively. The isolated copper oxide can be reduced easily; thus, peak α appears at a low temperature centered at ~470 K. When the copper combines with other coprecipitated metal oxides, metal interfaces, i.e., CuO/ZnO and CuO/ZrO_2, are formed, resulting in a higher reduction temperature for peak β[17]. Furthermore, the copper which has interacted with elements on the surface of HT during the CZZ-HT synthesis procedure presents an additional broad peak γ. In 1CZZ-HT, peaks α and β have appeared but cannot be easily discerned and peak γ occupies approximately 65.6% of the total H_2 consumption amount. Peaks α and β strengthen as the CZZ content in CZZ-HT samples increases, but peak γ gradually weakens until it is almost negligible in 7CZZ-HT. The trend reveals that the increased CZZ content in CZZ-HT promotes the formation of isolated copper oxide and CuO-ZnO-ZrO_2 compounds. Both peak α and β in 7CZZ-HT shift towards high temperature attributed to larger CZZ particles or copper agglomerates [43,44], which is consistent with the SEM results.

The essential role of basic sites has been acknowledged in methanol synthesis. According to previous reports in the literature, CZZ catalysts show three desorption peaks of CO_2 in the temperature range between 350 K and 523 K, corresponding to weak (peak α), moderate (peak β) and strong (peak γ) basic sites [45]. The HT consists of two broad desorption peaks centered at around 420 K (moderate basic sites, β') and 650 K (ultra-strong basic sites, γ') [46]. CO_2 adsorption on the ultra-strong basic sites occurs even at high temperature [29,47].

In CZZ-HT catalysts, therefore, two desorption peaks can be distinguished at ~470 K and ~660 K (Fig. 3). The former consists of

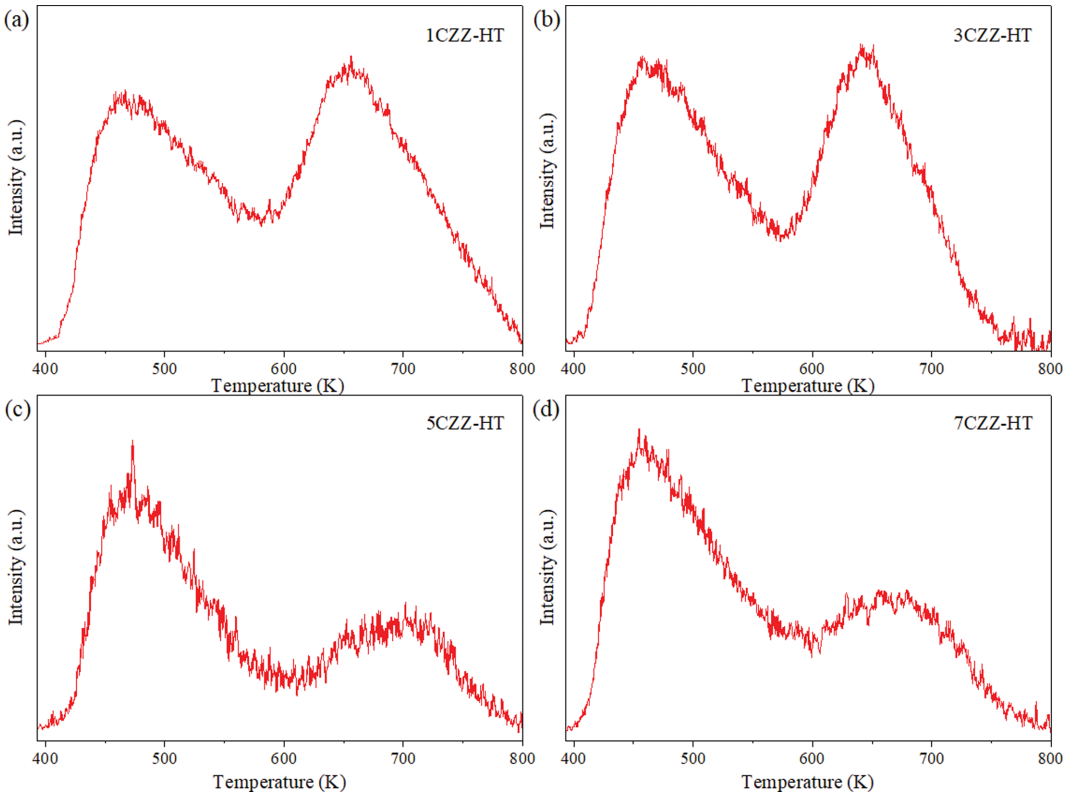

Fig. 3. Normalized CO_2-TPD profiles of (a) 1CZZ-TH, (b) 3CZZ-HT, (c) 5CZZ-HT and (d) 7CZZ-HT.

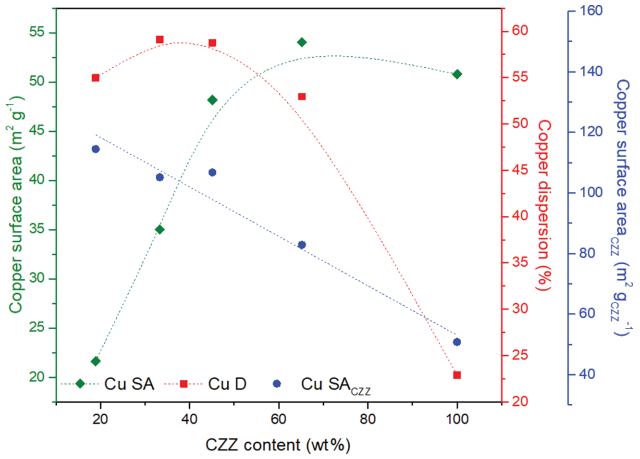

Fig. 4. Copper surface area and dispersion of samples with different CZZ content.

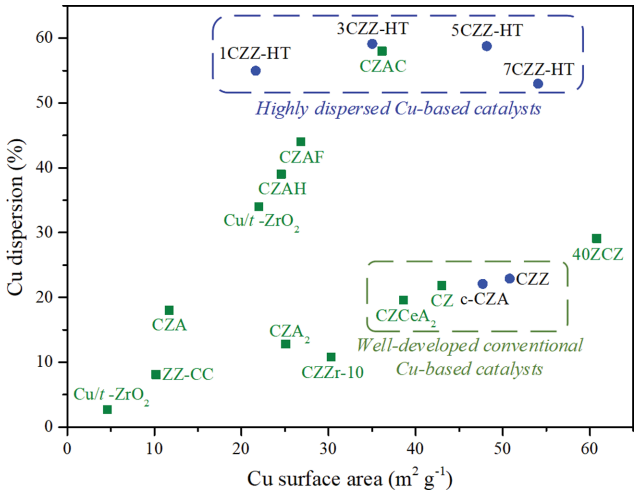

Fig. 5. Comparisons of copper surface areas and dispersions of catalysts in this work and literatures (blue circle - measured in this work; green square - catalysts reported in literatures [24-27,36,48-50]).

overlapped peaks of α, β and γ in CZZ and β' in HT, whereas the latter represents the ultra-strong γ' basic sites in HT. The presence of tailing peaks restricts further analysis of deconvolution, but it is obvious that the area of peak γ' decreases from 1CZZ-HT to 7CZZ-HT because the increasing CZZ content in samples weakens the ultra-strong basic sites resulting from HT.

In this work, copper surface area and copper dispersion were further measured by the N_2O titration method. As shown in Fig. 4, when the CZZ content is elevated, the Cu surface area per gram catalyst (green) rises dramatically with the CZZ content, reaching a peak of 54.1 m^2 g^{-1} in 7CZZ-HT but slightly dropping to 50.8 m^2 g^{-1} in pure CZZ. Contrarily, the Cu dispersion (red) declines rapidly with the CZZ content, among which the Cu dispersion of pure CZZ is only 22.9%, but both 3CZZ-HT and 5CZZ-HT reach ~59%. If we turn to the copper surface areas in unit active catalyst CZZ (blue), the CZZ-HT catalyst with low CZZ content presents high Cu surface area because copper can be well dispersed on the

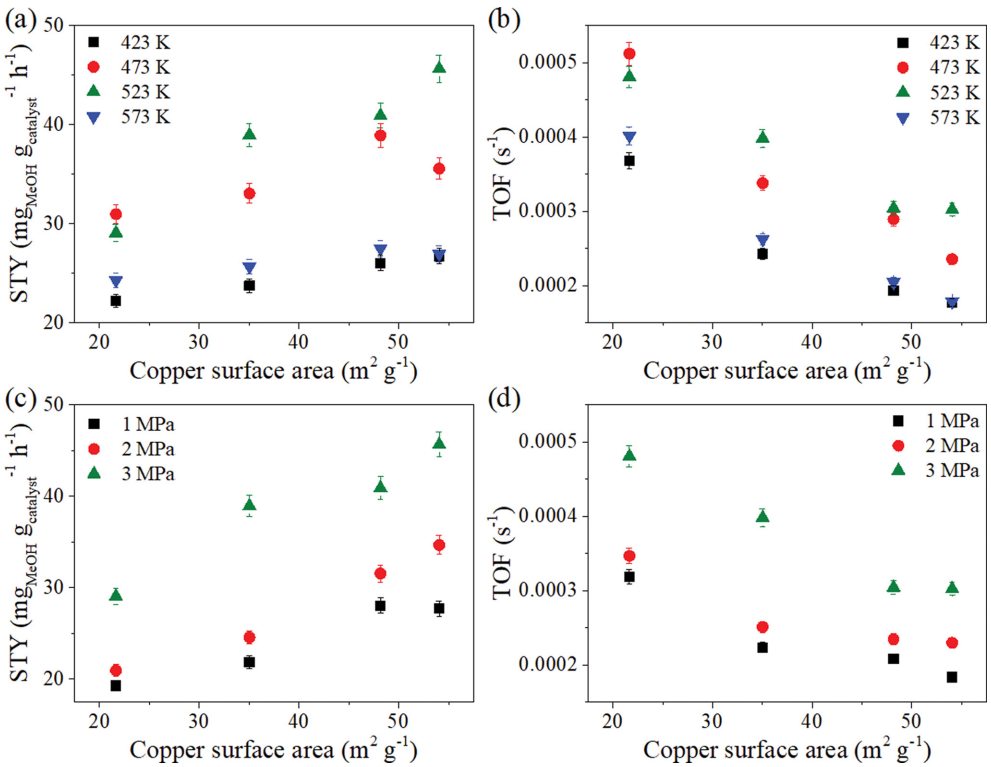

Fig. 6. Profiles of STY and TOF achieved by CZZ-HT catalysts at different reaction (a)-(b) temperatures at 3.0 MPa and (c)-(d) pressures at 523 K.

surface of the prepared catalyst. Alternatively, importing HT into the catalyst may enhance the efficiency of CZZ catalysts by forming more surface-active copper. Compared to pure CZZ, the copper surface area per gram CZZ and the copper dispersion of 5CZZ-HT increases by 1.1 times and 1.6 times, respectively.

Fig. 5 maps copper surface area and dispersion of the catalysts synthesized in this work and reported in the literature. It is observed that well-developed copper-based catalysts possess high copper surface areas of ~50 m^2 g^{-1} but low copper dispersions of ~23%. However, the highly dispersed copper-based catalysts prepared in this paper maintain both considerable copper surface areas and dramatic copper dispersion of ~55%, which would benefit their catalytic performance.

3. Catalytic Performance

At the given space velocity of ~3,000 mL $g_{catalyst}^{-1}$ h^{-1}, methanol STY and TOF of CZZ-HT samples are summarized in Fig. 6.

The overall STY of methanol increases with increasing of copper surface area at a fixed reaction temperature and a fixed pressure because the enriched active sites provide great potential to the reaction. The STY of methanol increases as the reaction temperature increases from 423 to 453 K, but the optimal STYs of methanol appear at the reaction temperature of 523 K as shown in Fig. 6(a). During the CO_2 hydrogenation, methanol synthesis and reverse water gas shift (RWGS) reaction take place simultaneously; however, the elevated temperature inhibits the exothermic reaction (methanol synthesis) but enhances the endothermic one (RWGS reaction), leading to low methanol STYs at 573 K [51]. The TOF follows a reverse trend to the STY as shown in Fig. 6(b). From Fig. 6(c), the STY of methanol can be elevated remarkably as the reaction pressure increases. The total mole numbers are reduced in the methanol synthesis reaction yet invariable in the RWGS reaction, so that the elevated pressure can benefit the production of methanol. In the aspect of TOF shown in Fig. 6(d), the same trend can be observed as discussed previously in Fig. 6(b).

With respect to the catalyst stability and regenerability, we selected the 5CZZ-HT as a representative to test it in long-time continuous reaction. It possesses similar copper surface area, yet higher copper dispersion compared with the commercial CZA catalyst. In the stability and regeneration experiment summarized in Fig. 7, the methanol STY stabilizes at approximately 38.5 mg_{MeOH} $g_{catalyst}^{-1}$ h^{-1} after 4 h of reaction. It slightly drops by 3.9% when the reaction proceeds for 96 h constantly, and it again reaches 40.6 mg_{MeOH} $g_{catalyst}^{-1}$ h^{-1} after regeneration in H_2 flow at 573 K for 6 h. The change in catalytic performance is basically neglectable if the experimental error is taken into consideration. In another stability analysis, the fresh and used 5CZZ-HT catalysts show same crystalline as confirmed by XRD patterns in Fig. 7. The used catalyst, despite the peak of sample holder at 2θ=~27°, exhibits almost identical crystal structure as the fresh one even 150 h of continuous reaction at 523 K and 3.0 MPa. Diffraction peaks of Cu^0 are still detectible in both samples at 2θ=43.3 and 50.4° (JCPDS 04-0836), and the HT remains in an amorphous state (by identifying broad peaks at 2θ=35.6, 43.4 and 62.8°), supplementing that there is no obvious deactivation. Therefore, the prepared 5CZZ-HT shows considerable stability and regenerability.

To better understand the quality of as-prepared CZZ-HT cata-

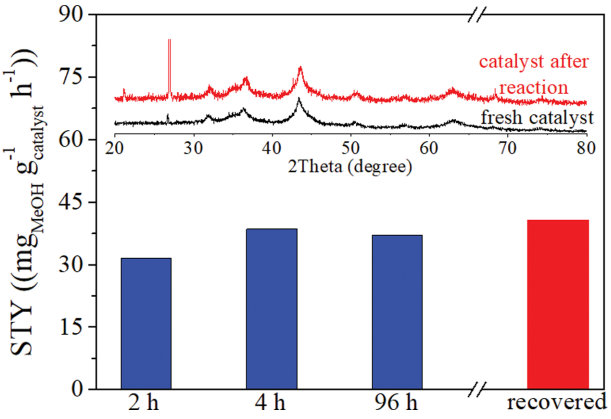

Fig. 7. Structure and property comparisons of fresh and reacted 5CZZ-HT (reaction temperature: 523 K, pressure: 3.0 MPa, space velocity: ~3,000 mL $g_{catalyst}^{-1}$ h^{-1}).

Table 3. Summary of catalytic performance of catalysts tested in this work

	P (MPa)	X_{CO2} (%)	S_{MeOH} (%)	Y_{MeOH} (%)	STY_{cat} [a]	STY_{Cu} [b]	S_{MeOH}/S_{CO}
5CZZ-HT	3.0	5.26	80.5	4.23	40.9	162.3	4.73
Activated HT	3.0	0	0	0	0	0	n.a.
c-CZA[c]	3.0	6.33	68.6	4.34	48.9	96.3	2.18
Pure CZZ	3.0	5.67	67.2	3.81	48.0	105.0	2.04
d-CZZ[d]	3.0	3.81	67.7	2.58	24.6	113.4	2.09
m-CZZ/HT[e]	3.0	4.71	72.8	3.43	37.0	160.1	2.68
5CZZ-HT	1.0	4.36	66.6	2.90	28.0	111.1	1.99
c-CZA[c]	1.0	3.56	28.9	1.03	11.6	22.8	0.41

[a]Methanol STY per gram catalyst (mg_{MeOH} $g_{catalyst}^{-1}$ h^{-1})
[b]Methanol STY per gram copper in the catalyst (mg_{MeOH} g_{Cu}^{-1} h^{-1})
[c]Commercial Cu-Zn-Al catalyst
[d]Diluted CZZ contains 21.7 wt% of Cu
[e]Physically mixed CZZ and HT powders (23.1 wt% of Cu). Refer to Reagents in SI for details about CZA, d-CZZ and m-CZZ/HT. All experiments listed in this table were conducted at the reaction temperature of 523 K and space velocity of ~3,000 mL $g_{catalyst}^{-1}$ h^{-1})

lysts, we compared them with a commercial copper-based catalyst for methanol synthesis. The results are summarized in Table 3. Basically, the isolate HT without CZZ does not show any catalytic characteristic, and the prepared pure CZZ catalyst presents similar STY to the commercial catalyst c-CZA, confirming reliable qualities of the homemade CZZ. For pure CZZ and diluted CZZ, the content of active components (CZZ in this work) correlates to the STY per gram catalyst linearly (see Fig. S6 in SI)[52], and the diluted CZZ shows an STY per gram CZZ of 51.7 $mg_{MeOH}\ g_{CZZ}^{-1}\ h^{-1}$ which is close to the pure CZZ (48.0 $mg_{MeOH}\ g_{CZZ}^{-1}\ h^{-1}$). Hence, the catalytic property is not improved by mixing quartz sand.

The synthesized CZZ-HT samples show dramatic property improvement by comparison. The typical 5CZZ-HT presents remarkable catalytic performance at 523 K and 3 MPa, i.e., an STY_{Cu} of 162.3 $mg_{MeOH}\ g_{Cu}^{-1}\ h^{-1}$ and a methanol selectivity of 80.5%. The STY_{Cu} of 5CZZ-HT exceeds that of c-CZA by 68.2% with similar methanol yield. It can also maintain attractive performance even when the reaction pressure drops to 1.0 MPa. Its S_{MeOH}/S_{CO} ratio is 4.73 at 3.0 MPa and 1.99 at 1.0 MPa, whereas these values observed in the commercial c-CZA are only 2.18 and 0.41. In another comparison of supported 5CZZ-HT and physically mixed m-CZZ/HT, there come visible property gaps especially in the methanol yield, so the 5CZZ-HT benefits from its structures apart from additional basic sites brought by the HT. Thus, the attractive behavior of CZZ-HT catalyst provides a promising approach to realize CO_2 hydrogenation under mild conditions, which will be significant for carbon capture, storage and utilization.

4. Impacts of HT for CO_2 Hydrogenation

It has been demonstrated previously that there are favorable changes in microstructure and catalytic property of CZZ-HT catalysts, i.e., surface areas, basic sites and copper dispersion, as HT is introduced as the carrier. Fig. 8(a) presents the HIM image of the reduced 5CZZ-HT catalyst (r5CZZ-HT). It primarily shows the same morphology to 5CZZ-HT obtained by SEM in Fig. 1(d). When it is magnified (Fig. 8(b)), complex pore systems are observed, where CZZ particles do not completely block pores of HT, resulting in efficient diffusion of reactants and products. Further magnification (Fig. 8(c)) shows the nanoparticles are highly dispersed. The HRTEM is also adopted to profile nanoparticles in r5CZZ-HT (Fig. 8(d)). It is observed that the average particle diameter is around 18 nm (Fig. 8(e)). Integrating characteristics discussed above, a schematic was plotted to help explain the observed results in Fig. 8(f). Specifically, reduced CZZ particles are loaded on the surface of the hydrotalcite to form microstructures.

As reported in previous theoretical works of CO_2 hydrogenation to methanol, the adsorption and dissociation of H_2 molecules take places on the surface of copper, while the adsorption of CO_2 occurs on the surface of ZnO-ZrO_2 or ZrO_2 [36,52,53]; the atomic hydrogen on the surface of copper is then removed by spillover to metal oxides and reacts with the carbon species which are adsorbed on the surface of these oxides, to form methanol [17,54,55]. There is a significant effect of basic sites on methanol selectivity (described in Fig. S7 in SI) that CO_2 can be adsorbed and activated on both β and γ basic sites of ZnO-ZrO_2, but the two types of basic sites lead to different reaction paths. Though formaldehyde ($*H_2CO$) is the major intermediate in both paths of methanol synthesis and CO generation, the $*H_2CO$ adsorbed on γ sites (strong basic sites) can be further hydrogenated to methanol but that on β sites (moderate basic sites) tends to form CO [45]. The basic sites of β and γ coexist in CZZs so that methanol and CO

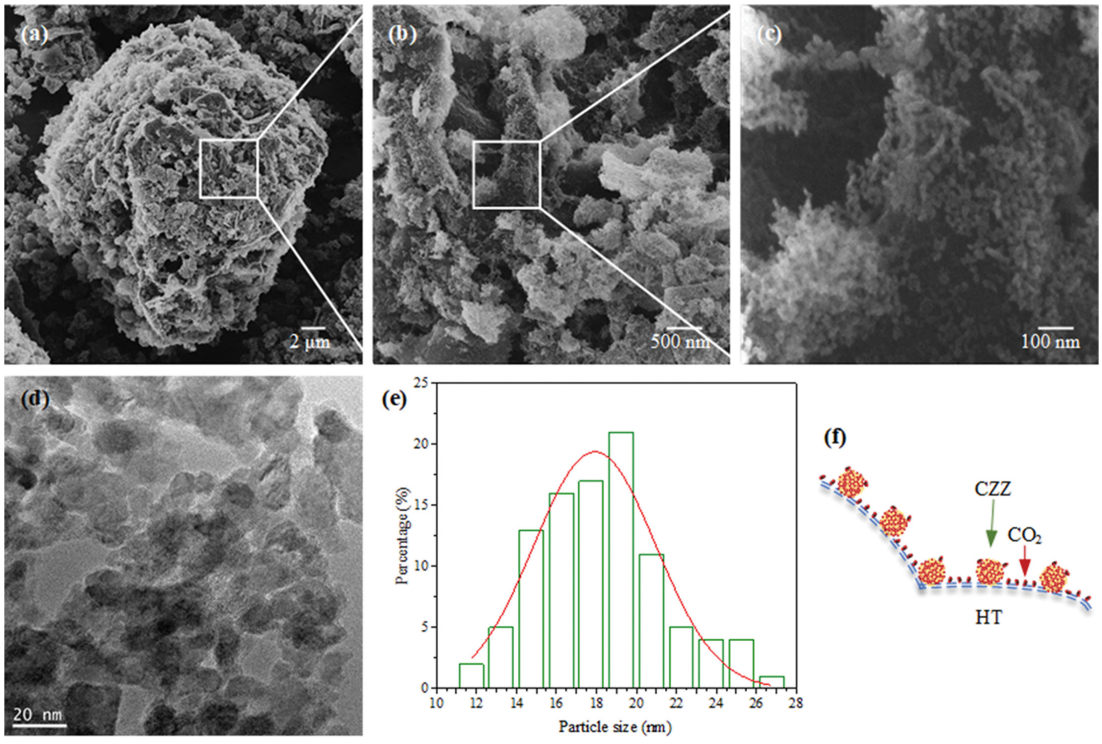

Fig. 8. (a)-(c) HIM images, (d) HRTEM image, (e) particle size distribution and (f) structure schematic of the r5CZZ-HT.

appear together in the product.

In CZZ-HT samples, the HT enhances CO_2 adsorption and activation on its surface at reaction temperatures because ultra- strong basic sites γ' exist in the HT. The CO_2 uptake of 5CZZ-HT is measured about 4.5 cm^3 (STP) g^{-1} at 473 K and 0.1 MPa, but that of pure CZZ is always below 1 cm^3 (STP) g^{-1}. Though the large amount of CO_2 adsorbed (*CO_2') on exposed sites of HT does not directly react with *H activated by Cu, its dynamic equilibrium of adsorption and desorption results in elevated surface CO_2 concentration directly adjacent to the active sites of ZnO-ZrO_2, enhancing CO_2 activation. The effect will be strengthened with reduced distance between CZZ and HT particles. This conjecture was confirmed by our previous work where the different particle sized commercial copper-based catalyst and HT were physically mixed and then were characterized. In this study, the prepared 5CZZ-HT can further reduce the distance between CZZ and HT particles than the physically mixed CZZ/HT so that it demonstrates improved catalytic activity (Table 3).

CONCLUSIONS

CuO-ZnO-ZrO_2-hydrotalcite (CZZ-HT) catalysts using HT as the carrier were prepared. It was found that the CZZ-HT catalysts contain CZZ nanoparticles anchored on the surface of HT, presenting significant improvement in BET surface area and basic sites. The introduced HT, in return, promotes the copper surface area and dispersion, ensuring the samples preferable properties to those well-developed conventional copper-based catalysts. Moreover, dramatic catalytic performance was attained with the modified catalysts for methanol synthesis via CO_2 hydrogenation. In the reaction at 523 K and 3.0 MPa, the sample 5CZZ-HT presents a CO_2 conversion of 5.26%, methanol selectivity of 80.5% and STY_{Cu} (based on the mass of active copper) of 162.3 mg_{MeOH} g_{Cu}^{-1} h^{-1}, which are much higher than the values achieved by physically mixed CZZ/HT, pure CZZ and even commercial catalyst c-CZA. Subsequent experimental and theoretical analyses supplement that the HT plays a crucial for the facilitated performance by regulating the microstructure and adjusting the basic sites.

ACKNOWLEDGEMENTS

The authors gratefully acknowledge the financial support of the China Scholarship Council (No. 201606080053), the University of Melbourne and the Natural Science Foundation of Liaoning Province (No. 2020-BS-053). We acknowledge the Monash X-ray Platform (MXP) for XRD measurements and Monash Centre of Electron Microscopy (MCEM) for SEM-EDX analyses. We also acknowledge the Materials Characterisation and Fabrication Platform (MCFP) at the University of Melbourne and the Victorian Node of the Australian National Fabrication Facility (ANFF) for the HIM characterizations.

SUPPORTING INFORMATION

Additional information as noted in the text. This information is available via the Internet at http://www.springer.com/chemistry/journal/11814.

REFERENCES

1. G. A. Olah, A. Goeppert and G. K. S. Prakash, *J. Org. Chem.*, **74**, 487 (2009).
2. A. Goeppert, M. Czaun, J.-P. Jones, G. K. Surya Prakash and G. A. Olah, *Chem. Soc. Rev.*, **43**, 7995 (2014).
3. S. Kar, J. Kothandaraman, A. Goeppert and G. K. S. Prakash, *J. CO_2 Util.*, **23**, 212 (2018).
4. F. Frusteri, M. Migliori, C. Cannilla, L. Frusteri, E. Catizzone, A. Aloise, G. Giordano and G. Bonura, *J. CO_2 Util.*, **18**, 353 (2017).
5. F. Jiao, J. Li, X. Pan, J. Xiao, H. Li, H. Ma, M. Wei, Y. Pan, Z. Zhou, M. Li, S. Miao, J. Li, Y. Zhu, D. Xiao, T. He, J. Yang, F. Qi, Q. Fu and X. Bao, *Science*, **351**, 1065 (2016).
6. Z. Wan, W. Wu, G. (Kevin) Li, C. Wang, H. Yang and D. Zhang, *Appl. Catal. A Gen.*, **523**, 312 (2016).
7. J. M. Thomas and K. D. M. Harris, *Energy Environ. Sci.*, **9**, 687 (2016).
8. M. Kong, Z. Liu, T. Vogt and Y. Lee, *Micropor. Mesopor. Mater.*, **221**, 253 (2016).
9. Y. Men, X. Fang, Q. Gu, R. Singh, F. Wu, D. Danaci, Q. Zhao, P. Xiao and P. A. Webley, *Appl. Catal. B Environ.*, **275**, 119067 (2020).
10. F. Studt, I. Sharafutdinov, F. Abild-Pedersen, C. F. Elkjær, J. S. Hummelshøj, S. Dahl, I. Chorkendorff and J. K. Nørskov, *Nat. Chem.*, **6**, 320 (2014).
11. N. Rui, Z. Wang, K. Sun, J. Ye, Q. Ge and C. Liu, *Appl. Catal. B Environ.*, **218**, 488 (2017).
12. X. Yang, S. Kattel, S. D. Senanayake, J. A. Boscoboinik, X. Nie, J. Graciani, J. A. Rodriguez, P. Liu, D. J. Stacchiola and J. G. Chen, *J. Am. Chem. Soc.*, **137**, 10104 (2015).
13. S. Kattel, P. J. Ramírez, J. G. Chen, J. A. Rodriguez and P. Liu, *Science*, **355**, 1296 (2017).
14. J. Schumann, T. Lunkenbein, A. Tarasov, N. Thomas, R. Schlögl and M. Behrens, *ChemCatChem*, **6**, 2889 (2014).
15. G. Bonura, M. Cordaro, C. Cannilla, F. Arena and F. Frusteri, *Appl. Catal. B Environ.*, **152**, 152 (2014).
16. M. K. Koh, Y. J. Wong, S. P. Chai and A. R. Mohamed, *J. Ind. Eng. Chem.*, **62**, 156 (2018).
17. B. Hu, Y. Yin, G. Liu, S. Chen, X. Hong and S. C. E. Tsang, *J. Catal.*, **359**, 17 (2018).
18. J. Xiao, D. Mao, X. Guo and J. Yu, *Appl. Surf. Sci.*, **338**, 146 (2015).
19. M. Tamura, T. Kitanaka, Y. Nakagawa and K. Tomishige, *ACS Catal.*, **6**, 376 (2016).
20. X. An, J. Li, Y. Zuo, Q. Zhang, D. Wang and J. Wang, *Catal. Lett.*, **118**, 264 (2007).
21. L. Liu and A. Corma, *Chem. Rev.*, **118**, 4981 (2018).
22. M. B. Boucher, B. Zugic, G. Cladaras, J. Kammert, M. D. Marcinkowski, T. J. Lawton, E. C. H. Sykes and M. Flytzani-Stephanopoulos, *Phys. Chem. Chem. Phys.*, **15**, 12187 (2013).
23. X. Guo, G. Fang, G. Li, H. Ma, H. Fan, L. Yu, C. Ma, X. Wu, D. Deng, M. Wei, D. Tan, R. Si, S. Zhang, J. Li, L. Sun, Z. Tang, X. Pan and X. Bao, *Science*, **344**, 616 (2014).
24. M. M.-J. Li, C. Chen, T. Ayvali, H. Suo, J. Zheng, I. Teixeira, L. Ye, H. Zou, D. O'Hare and S. C. E. Tsang, *ACS Catal.*, **8**, 4390 (2018).
25. C. Jeong and Y. W. Suh, *Catal. Today*, **265**, 254 (2016).
26. Z. Y. Ma, C. Yang, W. Wei, W. H. Li and Y. H. Sun, *J. Mol. Catal. A*

Chem., **231**, 75 (2005).
27. N. J. Venkatesha and S. Ramesh, *Ind. Eng. Chem. Res.*, **57**, 1506 (2018).
28. S. Abelló, F. Medina, D. Tichit, J. Pérez-Ramírez, J. C. Groen, J. E. Sueiras, P. Salagre and Y. Cesteros, *Chem. - A Eur. J.*, **11**, 728 (2005).
29. O. Aschenbrenner, P. McGuire, S. Alsamaq, J. Wang, S. Supasitmongkol, B. Al-Duri, P. Styring and J. Wood, *Chem. Eng. Res. Des.*, **89**, 1711 (2011).
30. N. D. Hutson, S. A. Speakman and E. A. Payzant, *Chem. Mater.*, **16**, 4135 (2004).
31. X. Fang, Y. Men, F. Wu, Q. Zhao, R. Singh, P. Xiao, T. Du and P. A. Webley, *J. CO_2 Util.*, **29**, 57 (2019).
32. S. Saha and S. B. Abd Hamid, *RSC Adv.*, **7**, 9914 (2017).
33. Y. Zhang, C. Chen, X. Lin, D. Li, X. Chen, Y. Zhan and Q. Zheng, *Int. J. Hydrogen Energy*, **39**, 3746 (2014).
34. X. Guo, D. Mao, G. Lu, S. Wang and G. Wu, *Catal. Commun.*, **12**, 1095 (2011).
35. A. Dandekar and M. A. Vannice, *J. Catal.*, **178**, 62 (1998).
36. F. Arena, G. Italiano, K. Barbera, S. Bordiga, G. Bonura, L. Spadaro and F. Frusteri, *Appl. Catal. A Gen.*, **350**, 16 (2008).
37. Y. Hua, X. Guo, D. Mao, G. Lu, G. L. Rempel and F. T. T. Ng, *Appl. Catal. A Gen.*, **540**, 68 (2017).
38. T. Phongamwong, U. Chantaprasertporn, T. Witoon, T. Numpilai, Y. Poo-arporn, W. Limphirat, W. Donphai, P. Dittanet, M. Chareonpanich and J. Limtrakul, *Chem. Eng. J.*, **316**, 692 (2017).
39. X. Dong, F. Li, N. Zhao, F. Xiao, J. Wang and Y. Tan, *Appl. Catal. B Environ.*, **191**, 8 (2016).
40. N. D. Hutson, S. a. Speakman and E. A. Payzant, *Chem. Mater.*, **16**, 4135 (2004).
41. S. Asthana, C. Samanta, A. Bhaumik, B. Banerjee, R. K. Voolapalli and B. Saha, *J. Catal.*, **334**, 89 (2016).
42. J. Y. Kim, J. A. Rodriguez, J. C. Hanson, A. I. Frenkel and P. L. Lee, *J. Am. Chem. Soc.*, **125**, 10684 (2003).
43. T. Witoon, J. Chalorngtham, P. Dumrongbunditkul, M. Chareonpanich and J. Limtrakul, *Chem. Eng. J.*, **293**, 327 (2016).
44. T. Witoon, N. Kachaban, W. Donphai, P. Kidkhunthod, K. Faungnawakij, M. Chareonpanich and J. Limtrakul, *Energy Convers. Manag.*, **118**, 21 (2016).
45. P. Gao, F. Li, H. Zhan, N. Zhao, F. Xiao, W. Wei, L. Zhong and H. Wang, *J. Catal.*, **298**, 51 (2013).
46. N. D. Hutson and B. C. Attwood, *Adsorption*, **14**, 781 (2008).
47. Z. Yong and A. E. Rodrigues, *Energy Convers. Manag.*, **43**, 1865 (2002).
48. A. G. Sato, D. P. Volanti, D. M. Meira, S. Damyanova, E. Longo and J. M. C. Bueno, *J. Catal.*, **307**, 1 (2013).
49. F. Frusteri, M. Cordaro, C. Cannilla and G. Bonura, *Appl. Catal. B Environ.*, **162**, 57 (2015).
50. S. Patel and K. K. Pant, *Chem. Eng. Sci.*, **62**, 5436 (2007).
51. L. C. Grabow and M. Mavrikakis, *ACS Catal.*, **1**, 365 (2011).
52. X. Guo, D. Mao, G. Lu, S. Wang and G. Wu, *J. Mol. Catal. A Chem.*, **345**, 60 (2011).
53. X.-M. Liu, G. Q. Lu, Z.-F. Yan and J. Beltramini, *Ind. Eng. Chem. Res.*, **42**, 6518 (2003).
54. T. Witoon, T. Numpilai, T. Phongamwong, W. Donphai, C. Boonyuen, C. Warakulwit, M. Chareonpanich and J. Limtrakul, *Chem. Eng. J.*, **334**, 1781 (2018).
55. K. Nishida, I. Atake, D. Li, T. Shishido, Y. Oumi, T. Sano and K. Takehira, *Appl. Catal. A Gen.*, **337**, 48 (2008).

Supporting Information

Highly dispersed Cu-ZnO-ZrO_2 nanoparticles on hydrotalcite adsorbent as efficient composite catalysts for CO_2 hydrogenation to methanol

Xin Fang*,, Yuhan Men**, Fan Wu**, Qinghu Zhao**, Ranjeet Singh**, Penny Xiao**, Liying Liu*, Tao Du*,†, and Paul A. Webley**,†**

*State Environmental Protection Key Laboratory of Eco-Industry, Northeastern University, Shenyang 110819, China
**Department of Chemical Engineering, The University of Melbourne, Parkville, VIC 3010, Australia
(*Received 22 September 2020 • Accepted 23 December 2020*)

Reagents

The commercial hydrotalcite (HT) of Pural MG50 (SASOL Germany GmbH) was chosen as the carrier for the catalysts. Its ratio of $MgO:Al_2O_3$ is reported 50 : 50. The BET surface area can exceed 200 $m^2\ g^{-1}$ after activation for 3 h at 823 K according to the manufacturer, and the BET surface area measured in this work after activation 4 h at 673 K was 195.2 $m^2\ g^{-1}$. Hence, the HT was fully activated before usage.

Metal nitrates, viz., $Cu(NO_3)_2{\cdot}2.5H_2O$, $Zn(NO_3)_2{\cdot}6H_2O$ and $ZrO(NO_3)_2{\cdot}xH_2O$, were supplied by Sigma-Aldrich, and the potassium carbonate (K_2CO_3) was offered by Ajax. Homemade deionized water was adopted for solution preparations. These reagents were all directly used without extra purification.

The quartz sand was also supplied by Sigma-Aldrich with the particle size of 50-70 mesh (diameter: 0.212-0.300 mm).

The commercial copper-based catalyst for methanol synthesis (CZA) which consisted of 63.5 wt% of CuO, 24.7 wt% of ZnO, 10.1 wt% of Al_2O_3 and 1.3 wt% of MgO was produced by Afar Aesar (product No.: 45776, Lot No.: C18W019). The pellet catalyst was ground and sieved to small particles (diameter within 0.2-0.5 mm) in this study. Before used in catalysis reactions, the catalyst particles were in situ reduced at 573 K for 6 h in pure H_2 (Coregas) flow.

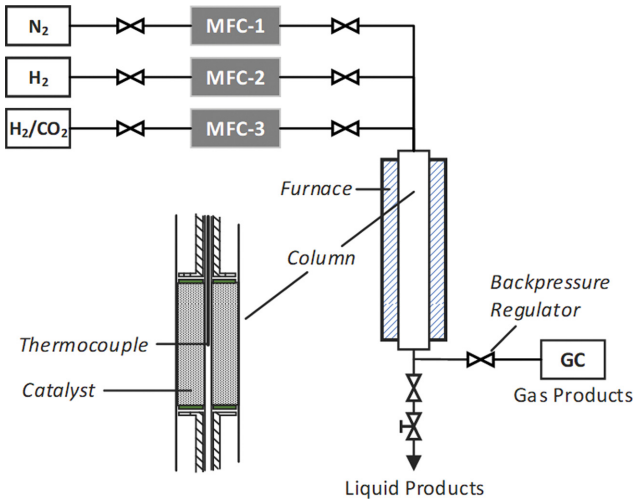

Fig. S1. Schematic of a fixed-bed micro reactor.

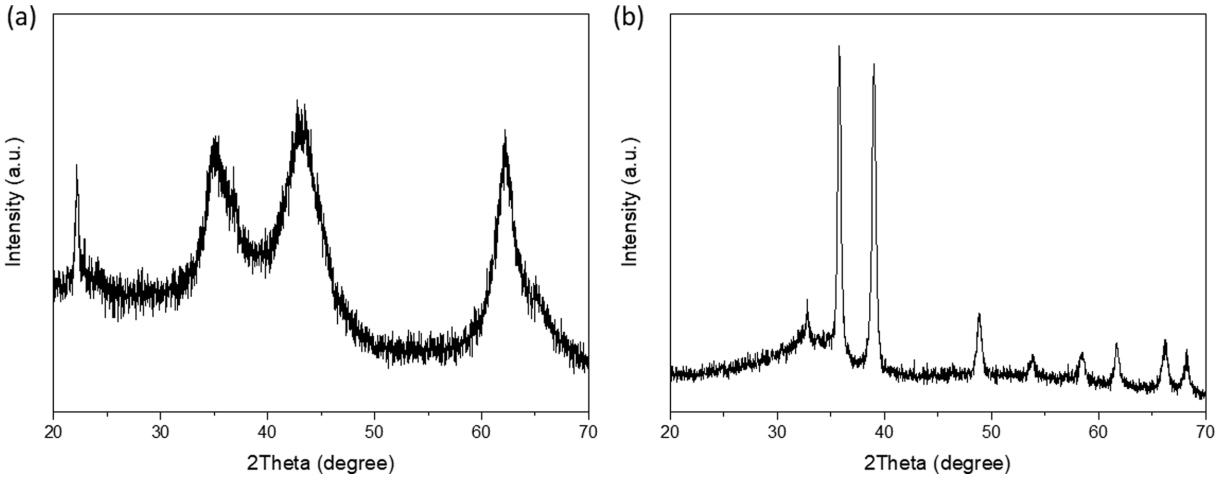

Fig. S2. XRD patterns of (a) amorphous HT and (b) pure CZZ. Despite of the peak of sample holder at 2θ=22°, the amorphous HT show three broad peaks at 2θ=35.6, 43.4 and 62.8° in (a). Sharp diffraction peaks of CuO (JCPDS 45-0937) and ZnO (JCPDS 36-1451) can be detected in pure CZZ in (b). Peaks of the tetragonal ZrO_2 (JCPDS 50-1089), are also observed but very weak [3].

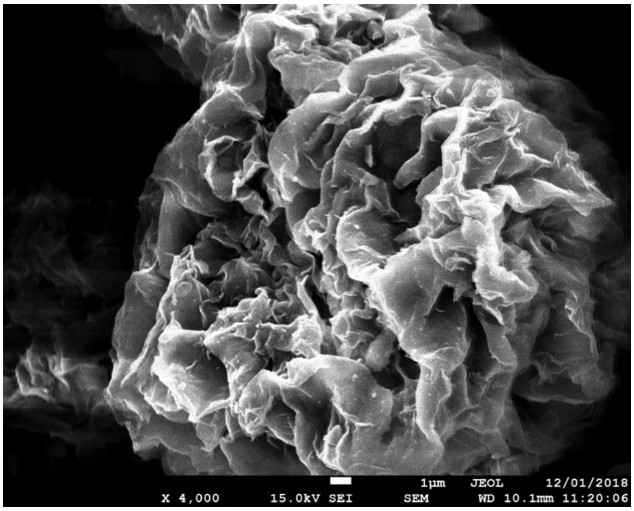

Fig. S3. SEM image of HT. It shows a nano-flower morphology with rich external surfaces.

The Cu-ZnO-ZrO_2 catalyst without HT carrier (CZZ) was synthesized by the conventional co-precipitation method. Typically, 1.2 M of K_2CO_3 solution was dropwise added in the ternary metal nitrate solution (Cu^{2+} 0.6 M, Zn^{2+} 0.3 M and Zr^{4+} 0.1 M) under continuously stirring. The slurry was then stirred for 2 h and aged for 1 h. After filtered, washed and dried at 393 K overnight, the precipitant was calcined at 673 K for 4 h to obtain CuO-ZnO-ZrO_2 powders. Before usage, the CZZ should be in situ reduced by H_2 at 573 K for 6 h.

The diluted CZZ was mixtures of CuO-ZnO-ZrO_2 catalyst (CZZ, prepared by the co-precipitation method) and quartz sand (non-porous), containing 47.56 wt% of CZZ and 52.44 wt% of quartz sand. This physically mixed catalyst possessed a similar percentage of CZZ content to the 5CZZ-HT catalyst (45.1 wt% measured and calculated from EDX data).

The mixed CZZ/HT was prepared by physically mixing CZZ and HT powders according to the mass ratio of CZZ : HT=50 : 50. The CZZ and HT used for physical mixing are very small in size (less than 0.1 mm in diameter) and tightly tableted together.

Micro-Reactor

Catalytic properties of catalysts were analyzed in a fixed bed micro reactor. There were three feed gas paths designed for N_2, H_2 and the mixed gas of H_2/CO_2, respectively. The flowrate of each inflow was individually controlled by the mass flow controller. The reaction column with the dimensions of Ø10 mm×L 500 mm could be heated uniformly by a three-stage furnace. As the effective height of catalyst layer in the column only occupied ~8% of the total length, the temperature of the catalysts could be perfectly maintained. The pressure in the system was adjusted by a backpressure regulator, after which the exiting gas was collected and measured by a gas chromatograph (GC7890B, Agilent). The schematic of this micro reactor was briefly presented in Fig. S1.

Reaction Parameter Calculations

CO_2 conversion (X_{CO_2}) was calculated as

$$X_{CO_2}=\left[1-\frac{F_{out}\times p_{out,\,CO_2}}{F_{in}\times p_{in,\,CO_2}}\right]\times 100\% \quad \text{(S1)}$$

where F_{in} was an inlet flowrate (NmL min^{-1}), F_{out} was an outlet flowrate (NmL min^{-1}), $p_{in,\,CO_2}$ and $p_{out,\,CO_2}$ were molar percentages (%) of CO_2 in feed gas and off-gas.

CO selectivity (S_{CO}) and methanol selectivity (S_{MeOH}) were calculated as

$$S_{CO}=\frac{F_{out}\times p_{CO}}{F_{in}\times p_{in,\,CO_2}-F_{out}\times p_{out,\,CO_2}}\times 100\% \quad \text{(S2)}$$

$$S_{MeOH}=\left[1-\frac{F_{out}\times (p_{CO}+p_{CH_4})}{F_{in}\times p_{in,\,CO_2}-F_{out}\times p_{out,\,CO_2}}\right]\times 100\% \quad \text{(S3)}$$

where p_{CO} and p_{CH_4} were molar percentages (%) of CO and CH_4 in off-gas. Only carbon-containing by-products of CO and CH_4

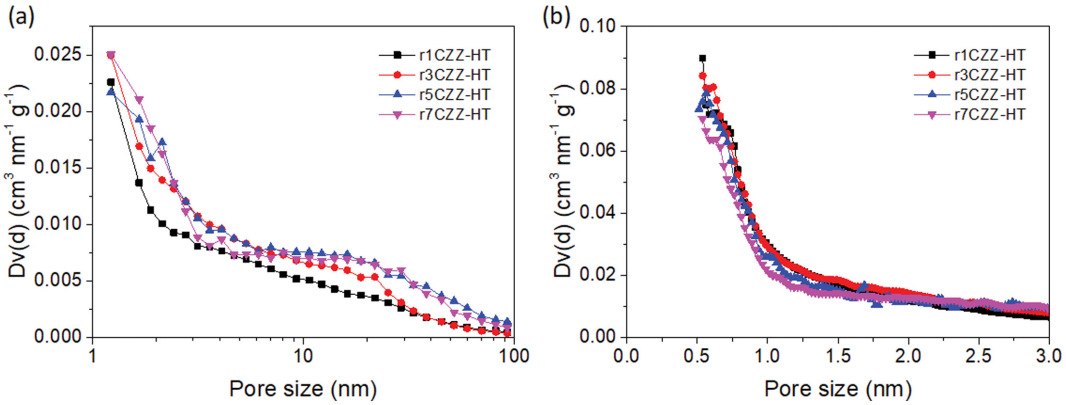

Fig. S4. Pore size distributions of reduced CZZ-HT catalysts ((a) BJH pore size distributions and (b) HK pore size distributions). In consideration of mesopores inferred by the BJH model (Fig. S4(a)), enlarged pore volumes can be observed generally when the CZZ content increases. These mesopores, derived from the interspace between CZZ particles, reflect the accumulation of CZZ on the surface of HT. In the micropore range between 0.5 and 1 nm shown in Fig. S4(b), the volumes increase slightly as the CZZ content in CZZ-HT samples decreases, because CZZ particles may block some micropores on the surface of HT. Consequently, the reduced 5CZZ-HT presents the largest pore diameter (14.40 nm) with a considerable BET surface area (119.5 m^2 g^{-1}), which will benefit reactant diffusion and product removal during chemical reactions.

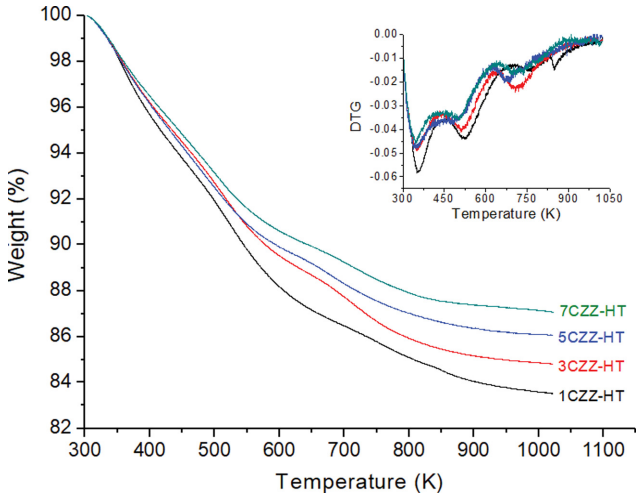

Fig. S5. TG and DTG analyses of 1CZZ-TH, 3CZZ-HT, 5CZZ-HT and 7CZZ-HT.

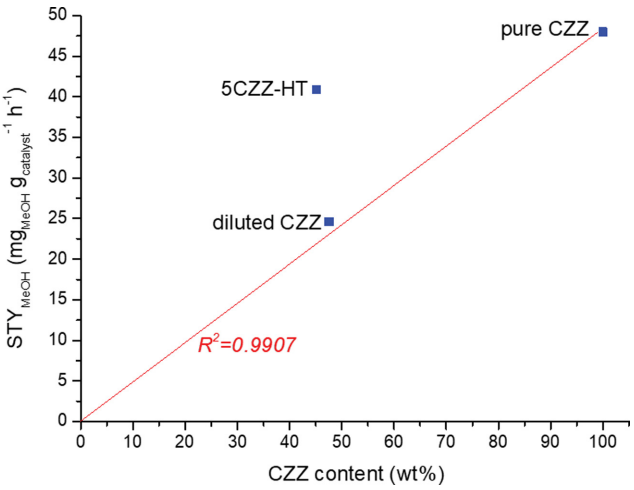

Fig. S6. Methanol STY comparisons of pure CZZ, diluted CZZ and 5CZZ-HT. The methanol STYs of pure CZZ, diluted CZZ and the zero point can be well fitted with a straight line (R^2= 0.9907), and hence the non-adsorptive quartz sand will not promote the methanol synthesis. The 5CZZ-HT, however, exhibits a much higher STY than the diluted CZZ with similar CZZ content. Therefore, the catalytic performances of CZZ have been improved efficiently by the HT.

were detected in both gas and liquid phases, so the carbon balance was calculated based on CO_2, methanol, CO and CH_4.

Methanol Space time yield per gram catalyst (STY_{cat}, mg_{MeOH} $g_{catalyst}^{-1}$ h^{-1}) was calculated as

$$STY_{cat} = \frac{m_{MeOH}}{m_{catalyst} \times t} \quad (S4)$$

where m_{MeOH} (g) was the mass of methanol produced, $m_{catalyst}$ (g) was the total mass of catalyst, and t (h) was the period of reaction.

Methanol space time yield per gram copper in catalyst (STY_{Cu}, mg_{MeOH} g_{Cu}^{-1} h^{-1}) was calculated as

$$STY_{Cu} = \frac{m_{MeOH}}{m_{catalyst} \times p_{Cu} \times t} \quad (S5)$$

where p_{Cu} (wt%) was the content of copper in catalyst.

The space velocity (SV, mL $g_{catalyst}^{-1}$ h^{-1}) was calculated as

$$\text{space velocity} = \frac{F_{in}}{m_{catalyst} \times t} \quad (S6)$$

Turnover frequency (TOF) was calculated as

$$TOF = \frac{STY_{cat} \times N_A}{MW_{MeOH} \times S_{Cu} \times A} \quad (S7)$$

where N_A was the Avogadro's number (6.023×10^{23}), MW_{MeOH} (g mol^{-1}) was the mole weight of methanol, S_{Cu} (m^2 g^{-1}) was the copper surface area and *A* was the number of copper atom on unit surface area (1.469×10^{19} atoms m^{-2}) [1].

Thermal Stability Analysis

Thermal stabilities of samples were analyzed by thermal gravimetric and differential thermal gravimetric (TG-DTG; TGA/SDTA851e, Mettler), where the ramping rate was set as 5 K min^{-1} from 303 to 1,023 K.

As shown in Fig. S5., the sample loses more weight if it contains more HT. The total weight losses from 303 to 1,023 K followed the order of 1CZZ-HT (16.5%)>3CZZ-HT (15.2%)>5CZZ-HT (13.9%)>7CZZ-HT (12.9%), which result from desorption, decomposition and destruction of HT [2]. These three impacts were easily observed by DTG presented in the subfigure. The first peak centred at ~344 K suggests the removal of adsorbed CO_2 and H_2O, the second one at ~510 K reflects dehydration and decarbonisation of HT, and the third at ~653 K is account of reversible destruction of double layer frameworks. The structure changes would become irreversible if the temperature continuously increases over 900 K, where the HT will be further transformed to spinelle. Since these peaks overlap each other, the factors listed above may work simultaneously for weight losses. Therefore, it's rational to con-

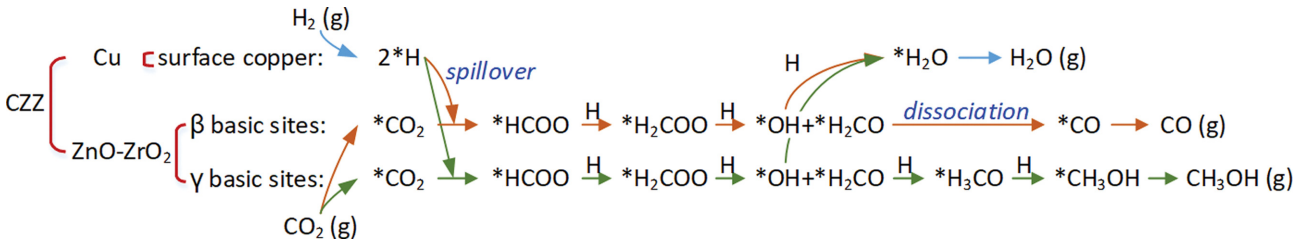

Fig. S7. Proposed reaction mechanisms of CZZ for CO_2 hydrogenation to methanol.

trol the reduction temperature under 600 K to protect the porous structures of samples.

REFERENCES

1. T. Witoon, J. Chalorngtham, P. Dumrongbunditkul, M. Chareonpanich and J. Limtrakul, *Chem. Eng. J.*, **293**, 327 (2016).
2. Y. Zhan, D. Li, K. Nishida, T. Shishido, Y. Oumi, T. Sano and K. Takehira, *Appl. Clay Sci.*, **45**, 147 (2009).
3. T. Witoon, T. Numpilai, T. Phongamwong, W. Donphai, C. Boonyuen, C. Warakulwit, M. Chareonpanich and J. Limtrakul, *Chem. Eng. J.*, **334**, 1781 (2018).